Impedance spectroscopic study on hybrid phthalocyanine/lead sulphide nanocomposite film

Zahra Khozaee[1], I. Chambrier[2], Lydia X. Sosa Vargas[2], Andrew N. Cammidge[2], and Asim. K. Ray[1,3]

[1]Centre of Materials Research, Queen Mary, University of London, Mile End Road London, E1 4NS, UK

[2]School of Chemistry, University of East Anglia, Norwich Research Park, Norwich, NR4 7TJ, UK

Abstract

A unique organic/inorganic nanocomposite of non-aggregated lead sulphide (PbS) quantum dots (QDs) dispersed within a spun film of non-peripherally octakis(hexyl) substituted metal-free phthalocyanine (C_6H_2Pc) has been prepared at room temperature by a simple and low-cost method. The frequency response of alternating current (AC) conduction in a 130 nm thick C_6H_2Pc/ PbS film sandwiched between the indium-tin-oxide (ITO) and aluminium (Al) electrodes is found to obey the universal power-law. The cryogenic study of AC conduction reveals that the correlated barrier hopping (CBH) model closely fits to the experimental data at temperatures below 240 K. The parameters obtained by fitting the CBH model point out that the hopping process cannot take place directly between neighbouring PbS QDs but involves the localised states within the matrix.

Keywords: Nanocomposite, discotic, macrocyclic, octahexylphthalocyanine, quantum dots, CBH modeling.

1.0 Introduction

Chemically and thermally stable, environmentally friendly non-toxic phthalocyanines (Pcs) are used in a range of applications from industrial pigments to photosensitizers as photodynamic agents in cancer therapy [1, 2,3]. The conjugated cyclic π-systems of eighteen electrons in the macrocyclic ring gives rise to unique semiconducting properties, offering tremendous scope of developing field effect transistors [4], solar cells of power conversion efficiency [5] and smart sensors for environmental pollution monitoring [6] and biodetection in ppb level [7]. Recently synthesised fluoroalkyl phthalocyanines are found to chemically robust, catalytically ~~self oxidation~~self-oxidation-resistant, n-type semiconductors which are not susceptible to electrophilic and nucleophilic outbreaks. These compounds therefore can be used as bioinspired catalytic agents in air and light [8]. Similarly, the size-dependent unique opto-electronic properties of crystalline semiconductor quantum dots (QDs) typically made of chalcogenides and phosphides of II to VI metals have attracted active research attention for their applications in nanoelectronics, optics and biological sciences [9,10]. In recent years, inorganic/organic hybrid nanocomposites incorporating semiconductor quantum dots into a phthalocyanine matrix have attracted considerable interest in fundamental and applied research because of their diverse fields of applications in sensors [11,12], displays [13, 14], photovoltaics [15, 16] and photonic devices [17, 18].

A unique organic/inorganic nanocomposite of lead sulfide (PbS) quantum dots (QDs) embedded in non-peripherally octakis(hexyl) substituted metal-free phthalocyanine (C_6PcH_2) has been prepared by a simple, one-step and low-cost method of 24 h long exposure of spin coated thin films of lead phthalocyanine derivative (C_6PcPb) to a H_2S environment in a sealed container. Transmission electron microscopic, X-Ray diffraction and UV-visible absorption studies have been performed on C_6PcPb films, C_6PcH_2/PbS nanocomposite and pristine C_6PcH_2 films [19]. The average PbS particle size is found to vary between 4.5 nm and 5.9 between obtained from TEM and XRD respectively. These values are much smaller than Bohr excitation radius of 18nm, indicating the formation of PbS quantum dots. Also, the value of 1.95eV is estimated for the band gap of PbS quantum dots. This is much larger than the bulk band gap of 0.41eV due to the quantum confinement. The average size of nanoparticles D and the volume fraction of nanoparticles in this hybrid were found to be 4.5 nm and 3%, respectively [20]. Organic/inorganic hybrid films of copper (II) phthalocyanine tetrasulfonic acid tetrasodium salt (CuPcTS) and tin oxide (SnO_2) have been fabricated using a simple soak-assembling process. These p-n heterojunctions show much improved performance at low

operating temperature of ~50℃ as NO_2 gas sensors in terms of high sensitivity and selectivity to ppb level [21].

In this work the frequency response of the conductivity of C_6PcH_2/PbS nanocomposite sandwiched between the ITO and Al electrodes is investigated by applying an AC signal with the amplitude of 0.1 V and sweeping frequency from 100 Hz to 1 MHz at temperatures ranging from 100 K to 293 K. In order to study the role of PbS quantum dots in the electrical properties of the nanocomposite device, the electrical properties of the pure matrix, C_6PcH_2, have been also investigated in the identical structural device and under the same ambient conditions. This dielectric relaxation spectroscopy, which involves the examination of AC electrical response over a wide frequency range, provides information on the conductivity of thin films of wide range materials in terms of structural homogeneity and stability considering relative contribution of grain, grain boundary and defect states [22]. Impedance spectroscopic measurements on nanocomposite containing cadmium selenide (CdSe) quantum dots dispersed into water-soluble polymer polyvinyl alcohol (PVA) matrix in the frequency and temperature ranges between 42Hz and 5MHz and 288 K and 523 K, respectively show the relaxation time of the nanocomposte is polydispersive. The non-Debye behavior of dielectric modulus is observed at relatively high frequencies [23].

2 Experimental

C_6PcPb and pristine C_6PcH_2 compounds, the synthesis of which was reported earlier, were used in this investigation [24]. Spin coated films of both compounds were deposited onto ultrasonically cleaned substrates from spreading solutions in toluene, concentration of 10 mg/ml, using a KW-4A spin-coater (Chemat Technology Inc.) operating at 1000 rpm for 30s. Under these conditions, deposited films were found to be approximately 130nm thick. from the measurement of surface variation present on the film by a DekTek surface profiler.

Following the procedure described before [19], the nanocomposite C_6PcH_2 /PbS/films were produced through a 24 h exposure of spin-coated films of C_6PcPb to a hydrogen sulphide (H_2S) environment in a sealed container. Under these conditions, the lead ion is removed and PbS nanoparticles are formed within a film of C_6PcH_2 as depicted in Figure 1(a).

The frequency response of the single-layered nanocomposite film sandwiched between an indium tin oxide (ITO) substrate and a 60nm thick evaporated aluminium (Al) counter electrode, as shown in Figure 1(b), was obtained using Autolab potentiostat PGSTAT30. The admittance Y were measured by applying an AC signal with amplitude of 0.1 V. The

frequency was swept from 100 Hz to 1 MHz at different temperatures between 100K and 293 K.. The effective area of the devices was estimated to be 4.5 mm^2 from the overlap between top the Al and the bottom ITO electrodes. A similar sandwich structure device was also fabricated using spun C_6PcH_2 films as the semiconducting active material.

A continuous-flow cryostat, made by Oxford Instruments, was employed to measure the temperature-dependency of the electrical characteristic of the devices. The cryostat was operated on the dynamic mode by circulating nitrogen gas around the device holder. During the experiment, the cryogen liquid was continuously transferred from a cryogen container to the cryostat through a transfer tube. The temperature was controlled using an Oxford Instrument ITC503 temperature controller and the temperature was measured via a temperature sensor near the device holder. The rate of cryogen flow was controlled manually. The temperature range used in this study was between 293 K and 100 K.

3. Results and discussion

Experimental results were presented structures along with the evaluation of values of relevant physical parameters.

3.1 AC Conductivity

The real and imaginary parts of admittance, Y' and Y'' respectively, are obtained by applying an alternating field to the sandwich structure devices where $Y = Y' + iY''$. Given the geometry of the devices, the AC conductivity is then estimated from the real part of admittance which is known as conductance, $\sigma_{AC} = \frac{d}{A}Y'$, where d is the thickness of the films, $d^{Pc} = 100$ nm and $d^{NC} = 130$ nm, and A is the effective area of the devices $A = 4.5\ mm^2$. The superscripts Pc and NC are used for identifying the quantities corresponding to C_6PcH_2 and C_6PcH_2/PbS nanocomposite, respectively. Figures 2(a) and 2(b) show the logarithmic plots of frequency-dependence of the conductivity $\sigma_{AC}(\omega, T)$ for C_6PcH_2/PbS and C_6H_2Pc devices, respectively. The AC conductivity σ_{AC} of the nanocomposite C_6PcH_2/PbS film is found to be higher than that of C_6PcH_2 device by about two orders of magnitude. However, the behaviour of AC conductivity with respect to frequency $f\ (= \frac{\omega}{2\pi})$ and temperature T are similar for both devices. Significant increase in σ_{AC} has been reported for optimized polyaniline-nickel ferrite nanocomposite over polyaniline due to the formation of p-n type heterojunction at the interface between n-type nickel ferrite and p-type polyaniline [25].

At a given temperature T, $\sigma_{AC}(\omega, T)$ increases monotonically by increasing frequency from 10^2 Hz to 10^6 Hz. $\sigma_{AC}(\omega, T)$ is temperature-dependent and decreases by lowering temperature down to T=100 K. A similar frequency dispersion conductivity is reported for the nanocomposite cadmium selenide sulphide/zinc sulphide quantum dots dispersed in 4-pentyl-4-cyanobiphenyl nematic liquid crystalline material [26]. However, in disorder systems with lack of band-type conduction, the AC conductivity σ_{AC} is frequency-dependent, universally observed to follow the universal power-law equation [27]:

$$\sigma_{AC}(\omega, T) = \sigma_{DC}(T) + A\omega^s \qquad (1)$$

where $\sigma_{DC}(T)$ is the DC conductivity when $\omega \rightarrow 0$, A is prefactor and s is the frequency exponent. Both A and s are weakly dependent on temperature. The power-law frequency-dependence is mostly observed in the frequency range from ~ 1 Hz to 10 GHz where the quantum and phonon effects become dominant [28]. The values of s obtained for C_6PcH_2 and C_6PcH_2/PbS nanocomposite are tabulated in Table 1.

The slope of $\sigma_{AC}(\omega, T)$ with respect to temperature T is plotted in Figure 2(c). The graphs can be approximately divided into low and high frequency regions corresponding respectively to the frequency below and above 10^4 Hz. The values of slope s for f <10^4 Hz are less than unity, while they exceed unity at frequencies higher than 10^4 Hz. This type of behaviour is commonly reported for disordered semiconductors [29]. Values of slope below unity indicate that the frequency-dependence of the conductivity of both devices can be well-described by the universal power-law in Equation (1) above.

3.2 Conduction mechanism

The frequency response of the materials has been analysed in order to determine the dominant AC conduction mechanism. The increase of s with decreasing temperature T is consistent with the correlated barrier hopping (CBH) model in which the relaxation process occurs by hopping of charges between pair of localised states [30]. Similar conduction mechanism is reported for 8mm in diameter and 1.1mm in thickness of rectangular pellets of newly synthesized inorganic-organic tetrapropylammonium tetrachloferrate nanocomposite at temperature between 313K and 388 K over the frequency range from 10^3Hz to 10^7 Hz [31]. The consistency of the CBH model for both σ_{AC}^{Pc} and σ_{AC}^{NC} is further investigated by fitting the following CBH equation (2) for both films:

$$\sigma_{AC} = \frac{\pi^3}{24} N^2 \epsilon \varepsilon_0 \omega R_\omega^6 \qquad (2)$$

and

$$R_\omega = \frac{e^2}{\pi \epsilon \varepsilon_0 (W_m + kT\, ln(\omega \tau_0))}. \qquad (3)$$

Where R_ω, W_m and N represent hopping distance, maximum barrier height and density of hopping sites, respectively [32]. Values of these variables are found through the fitting process. The other parameters are characteristic relaxation time which is assumed to be equal to the inverse of phonon vibration frequency, $\tau_0 = 10^{-13}$s. The value of dielectric constant, ε, is found to be 5 and 6.2, respectively, for C_6PcH_2 and C_6PcH_2/PbS nanocomposite. Figures 3 and 4 depict the results of the fitting for both C_6H_2Pc and the C_6H_2Pc/PbS nanocomposite, respectively. The Arrhenius plots show the temperature-dependence of the AC conductivity in the form of σ_{AC} vs. $1000/T$ with the frequency as parameters. The plots of temperature-dependence of the exponent s (s vs. T) have also been included for both structures for the sake of clarity. The theoretical values of s are calculated using equation [33]

$$s_{CBH}(\omega, T) = 1 - \frac{6kT}{W_m + kT\, ln(\omega \tau_0)} \qquad (4)$$

The typical values are calculated at the fixed frequency of 10^3 Hz. The frequency dispersion of s is very weak and negligible (lower than %1 and %1.3 for the obtained values of W_m^{Pc} and W_m^{NC}, respectively. It is to be noted from the fitting results that the CBH model is well fitted to the AC conductivity of both C_6PcH_2 and the C_6PcH_2/PbS samples at temperatures lower than 240 K. For higher temperatures (T>240), the temperature-dependence of σ_{AC}^{Pc} and σ_{AC}^{NC} is much stronger than the prediction from the CBH model.

The obtained values of W_m and N for both materials have been listed in Table 1. The value of W_m for the C_6PcH_2/PbS nanocomposite is smaller than that of the C_6PcH_2 while N of the C_6PcH_2/PbS nanocomposite is larger than that of C_6PcH_2 by a factor of 6. These observations suggest that the incorporation of the PbS QDs in C_6PcH_2 introduces new hopping sites with smaller binding energy, making a dominant contribution to the AC conduction of the nanocomposite, at least for T<240 K. Some possible sources of the new hopping sites can be morphological defects introduced to the matrix by inclusion of the PbS QDs, surface states and dangling bonds of the PbS QDs are also probable contributors . Using the relation of R_ω, the most probable hopping length in the nanocomposite is found to be 0.69 ± 0.1 nm.

The average distance between centers of two neighboring particles, $\tilde{r}$, is calculated to be ~11.7 nm using equation in the form [34]:

$$\tilde{r} = (6x/D^3\pi)^{-1/3} \qquad (5)$$

using $D = 4.5\ nm$ and $x = 3\%$ The hopping length in the nanocomposite, 0.69 ± 0.1 nm, is much smaller than the distance $\sim 11.7\ nm$ between the PbS QDs in the nanocomposite, indicating there may not be any direct hopping between two neighboring quantum dots.

3.3 Dielectric dispersion

The relative dielectric constant of the device is calculated using the expression $\varepsilon = \frac{d}{\varepsilon_0 A}\frac{Y''}{\omega}$ [35]. Figure 5 shows the frequency-dependence of the dielectric constant of C_6PcH_2 and C_6PcH_2/PbS nanocomposite device. The nanocomposite exhibits stronger frequency dispersion compared to the pure matrix. This may be due to the presence of interfacial polarisation at the interface between the PbS QDs and the matrix. The interfacial polarisation typically observed in heterojunction systems when the polarisation abilities of the phases are different, and it is mainly dominant at the low frequency region [36]. The frequency- and temperature-dependence of ε in both devices are becoming weaker with decreasing temperature and nearly disappeared at around 200 K. The value of dielectric constant at very high frequencies, near optical frequencies, corresponds only to electronic polarisation of materials (displacement of electrons around nuclei) rather than any other polarisation such as interfacial, dipole orientational and/or ionic polarisation. Lowering the temperature can also reduce the effect of the orientational polarisation. Accordingly, the high-frequency dielectric constant can be determined from the saturation value of ε at very high frequency and low temperature. Values of the dielectric constant at the highest attained frequency and lowest temperature is found to be ~5 and ~6.2 corresponding to C_6PcH_2 and the C_6PcH_2/PbS nanocomposite, respectively. An increase of the dielectric constant has been reported for of hybrid material consisting of carbon nanotubes-copper phthalocyanine [37]. These materials may be utilized in High memory cell dielectrics, gate dielectrics, and passive components.

4. Conclusion

Impedance spectroscopic measurements have been made 100 Hz to 1 MHz at different temperatures between 100K and 293 K on hybrid nanocomposite C_6PcH_2/PbS films. A simple,

one-step method is employed to produce, at room temperature, a single layer of organic-inorganic nanocomposite containing non-aggregated lead sulphide (PbS) quantum dots (QD) embedded in a 130nm thick solution processed film of the organic semiconductor C_6PcH_2 on indium tin oxide (ITO). The AC conductivity of the phthalocyanine/lead sulphide nanocomposite is frequency-dependent following the universal power-law in frequency ranging from 100 Hz to 1 MHz. However, for $f < 10^4$ Hz and temperature $T < 240$ K, the charge relaxation is found to occur by hopping between correlated barrier hopping between localised states mainly at $T < 240$ K. By fitting data to the correlated barrier hopping (CBH) model, the hopping length was found to be 0.69 ± 0.1 nm which is much smaller than the estimated distance between the PbS QDs, ~ 11.7 nm. This indicates that the direct hopping between the neighboring QDs is very unlikely, but it involves the localised states within the matrix.

References

1. . Chen J., Zhu C. J.,. Xu Y, Zhang P. W . and Liang T. X., *Curr. Org. Chem* 2018; **22(5):** 485-504
2. Woehrle D, Schnurpfeil G., Makarov S.G., Kazarin A. and Suvorova O. N. *Macroheterocyles* 2012; **5(3):** 191-202.
3. Claessens C. G., Hahn U. and Torres, T., *Chem. Rec.*, 2008; **8(2):** 75-97.
4. Melville O. A., Grant T. M., Mirka B. Boileau N. T., Park J. and Lessard B. H. *Adv. Electron. Mater*. 2019, **5(8): Article Number:** 1900087
5. Zhang S., Hu Z. L., Zhang J., Jia X. G. , Jiang J., Chen Y. Q., Lin B. C., Jiang H., Fang B. J., Yuan N. Y. and Ding J. N. *J. Power Sources.* 2019, ,**438**: **Article Number:** 226987.
6. Zeng Z. R., Fang X., Miao W., Liu Y., Maiyalagan T. and Mao S. *ACS Sens.* 2019; **4(7)**: 1934-1941
7. de Albuquerque Y. D. T. and Ferreira L. F., *Anal. Chim. Acta* 2007: **596(2)**: 210-221.
8. Carrion E. N., Loas A., Patel H. H., Pelmus, M., Ramji K. and Gorun S. M., J. *Porphyr. Phthalocyanines* 2018, **22(5)** 371-397
9. Chand S., Thakur N., Katyal S. C., Barman P. B. Sharma V. and Sharma P., *Sol. Energy Mater. Sol. Cells* 2017;**168:** 183-200
10. Li H., Jia C., Meng X. W. and Li H. B., *Nanocrystals.* 2017; 6: **Article Number:** 652
11. Bouvet M., Gaudillat P. and Suisse J. M., *J. Porphyr. Phthalocyanines* 2013, **17(10);** 913-919

12. Lu L., Zhu Z. W. and Hu X. Q., *Trends Food Sci. Technol.* 2019, **90:** () 100-110 .
13. Yuan L. T. Pan L., Jia K., Liu Y. Y., Huang Z. F., Huang Y. M and Liu X. B., *Synth. Met.* 2016, **218:** 9-18.
14. Mandali S., Iglesias M. G.., Ince M., Torres T. and Tkachenko N. V., *ACS Omega* 2018, **3(8):** 10048-10057.
15. Guchhait A., Das S., Ray S. K. and Pal A. J., *Nanosci. Nanotechnol. Lett.* 2013, **5(1):** () 13-18
16. Khurana P., Thatai S., Chaure N. B., Mahamuni S. and Kulkarni S, *Thin Solid Films* 2014, **565**;202-206
17. Wang J., Zhang Y. J., Ye J. Q. and Jiang Z., *Luminescence* **2017, 32(4)**: 573-580.
18. Sanusi K., Khene S. and Nyokong T. ,. *Opt. Mater*. 2014, **37**:572-582.
19. Nabok A. V., Ray A. K., Cook M. J., Burnham P. M., Iwantono, Yanuar H., Simmonds M. and Basova T. V., *IEEE Trans. Nanotechnol. 2004*, 3(3):388-394.
20. Khozaee Z., Sosa-Vargas L., Cammidge A. N., Cook M. J. and Ray A. K., *Mater. Res. Express* 2015, **2:** 096305.
21. Liu Z. W., Yang X., Huo L. P., Tian X., Qi T. J., Yang F., Wang X. F., Yu K., Ma F. G., and Sun J., *Sens. Actuator B-Chem*.2017; **248:** 324-331.
22. Long A. R. , Advances in Physics 1982, **31(5**): () 553-637.
23. Tyagi C. and, Devi A., *J. Nanoelectron. Optoelectron.* 2019, **14(1)::**128-135
24. Burnham P.M., Chambrier I ,. Hughes D. L., Isare B, Poynter R.J., Powell A.K. and Cook M.J, *J. Porphyr. Phthalocyanines* 2006, **10**(9-10):, 1202-1211.
25. Megha R., Ravikiran Y. T., Kumari S. C. V. and Thomas S. ,. *Appl. Phys. A-Mater. Sci. Process* 2017, **123(4**) **Article Number:** 245
26. Kocakulah G., Onsal G., Goksen K., Ercan I. and Koysal O., *Physica B* 2018, **550:** 47-59.
27. Jonscher A.K., *Universal Relaxation Law* (Chelsea Dielectric Press, London, 1996)
28. Elliott S. R., *Adv. Phys.*. 1987, 36(2):., 135-218.
29. Jonscher A.K., *Dielectric relaxation in solids*, Chelsea Dielectrics Press Ltd, London, 1983.
30. Long A.R. *Adv. Phys.*, **1982, 31:** 553-637,
31. Ben Brahim K., Ben Gzaiel M., Oueslati A., Hlel F. and Gargouri M., *Mater. Res. Bull.* 2019, 118:**Article Number:** 110505.
32. Hill R. M. and Jonscher A. K., *J. Non-Cryst. Solids* **1979, 32(1-3):** 53-69 .
33. Mott N.F. and Davis E.A., *Electronic Process in Non-Crystalline Materials*, 2nd Edn. (Clarendon Press, Oxford, 1979, 32–37

34. Choudhury K. R., Samoc M, Patra A. and Prasad P. N., *J. Phys. Chem. B* 2004, **108** (5): 1556-1562.

35 Gould R. D., *Coord. Chem. Rev.* 1996, **156**: 237-274.

36. S. O. Kasap, *Principles of electronic materials and devices*, McGraw-Hill, 2006.

37 Pu Z. J., Chen L,, Tong L. F., Long Y., Huang X and Liu X. B, *Mater. Lett.* 2013, **109**, 116-119

Figure captions

Figure 1 (a) Scheme of the formation of the lead sulphide (PbS) quantum dots and metal free 1,4,8,11,15,18,22,25-octakis(hexyl)phthalocyanines from the corresponding lead phthalocyanines (C_6PbPc) (b) Sandwich device structure of C_6PcH_2/PbS nanocomposite between ITO and Al electrodes.

Figure 2. The frequency dispersion of AC conductivity σ_{AC} of (a) C_6PcH_2 and (b) C_6PcH_2/PbS at different temperatures. The dash lines are the best-fitted lines to the plots for region below 10^4 Hz. (c) the dependence of exponent s on temperature T (circle and square symbols for f $\leq 10^4$Hz and f $> 10^4$Hz, respectively) The error of the listed values is not more than 2%.

Figure 3. Fitting the CBH model to the experimental data of C_6PcH_2 device presenting by (a) temperature-dependence of the $\boldsymbol{\sigma_{AC}}$ conductivity (b) temperature-dependence of exponent *s*.

Figure 4. Fitting the CBH model to the experimental data of C_6PcH_2/PbS device presenting by (a) temperature-dependence of the AC conductivity (b) temperature-dependence of exponent *s*.

Figure 5. Frequency dispersion of dielectric constant of (a) C_6PcH_2 and (b) C_6PcH_2/PbS nanocomposite.

Table 1. Parameters applied for fitting the CBH model to the AC conductivity of the materials.

	W_m (eV)	N (m^{-3})	ε	τ_0 (s)
C_6PcH_2	2	7.3×10^{25}	5	10^{-13}
C_6PcH_2/PbS	1.8	4.5×10^{26}	6.2	10^{-13}

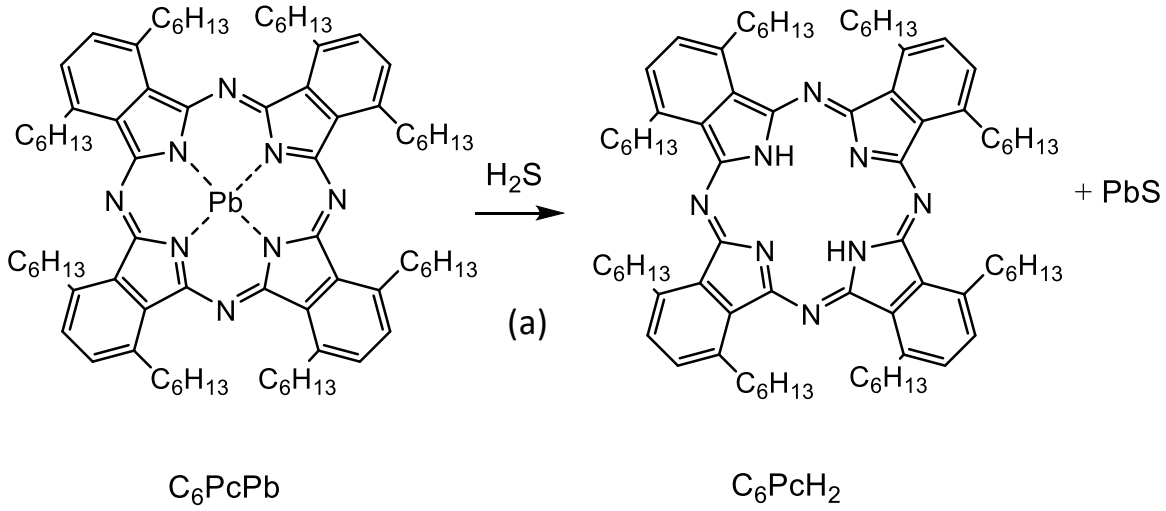

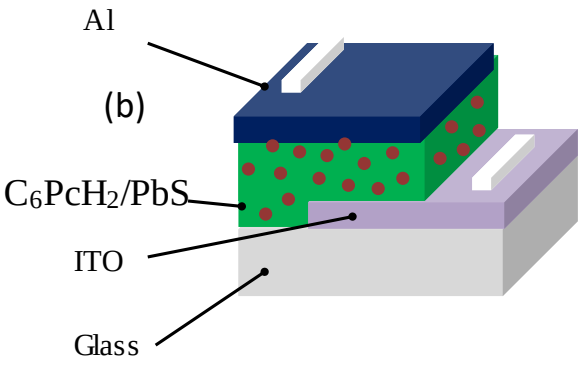

Figure 1 (a) Scheme of the formation of the lead sulphide (PbS) quantum dots and metal free 1,4,8,11,15,18,22,25-octakis(hexyl)phthalocyanines from the corresponding lead phthalocyanines (C_6PbPc) (b) Sandwich device structure of C_6PcH_2/PbS nanocomposite between ITO and Al electrodes.

(a)

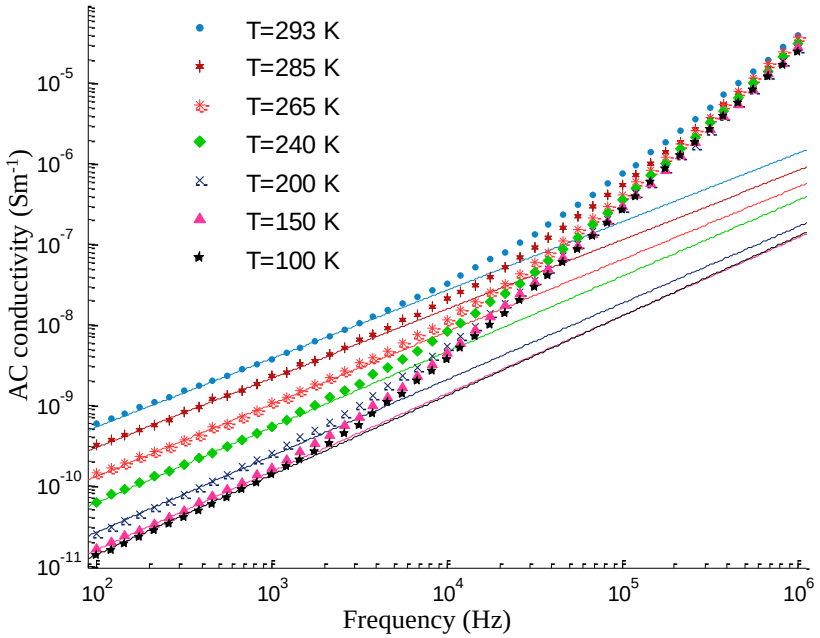
T=293 K
T=285 K
T=265 K
T=240 K
T=200 K
T=150 K
T=100 K
AC conductivity (Sm-1)
Frequency (Hz)

(b)

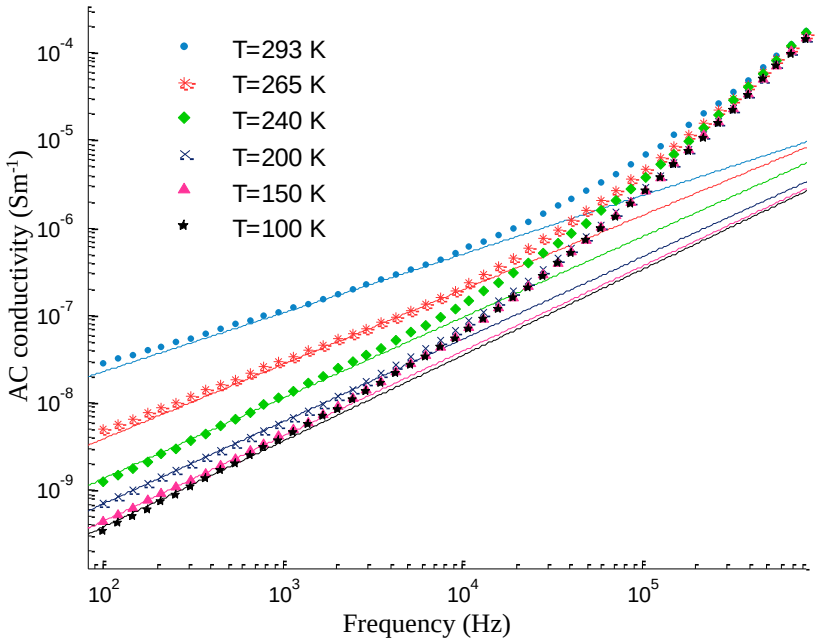
T=293 K
T=265 K
T=240 K
T=200 K
T=150 K
T=100 K
AC conductivity (Sm-1)
Frequency (Hz)

Freque

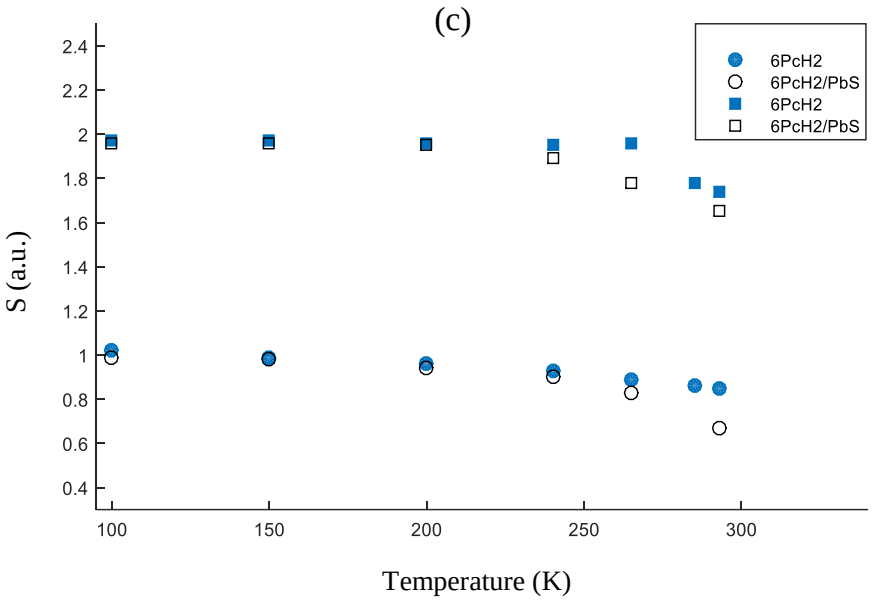

Figure 2. The frequency dispersion of AC conductivity $\boldsymbol{\sigma_{AC}}$ of (a) C_6PcH_2 and (b) C_6PcH_2/PbS at different temperatures. The dash lines are the best-fitted lines to the plots for region below 10^4 Hz. (c) the dependence of exponent $\boldsymbol{s}$ on temperature $\boldsymbol{T}$ (circle and square symbols for $\mathbf{f \leq 10^4 Hz}$ and $\mathbf{f > 10^4 Hz}$, respectively) The error of the listed values is not more than 2%.$\boldsymbol{\sigma_{AC}}$**sTf** $\leq$ **10^4Hzf $>$ 10^4Hz**

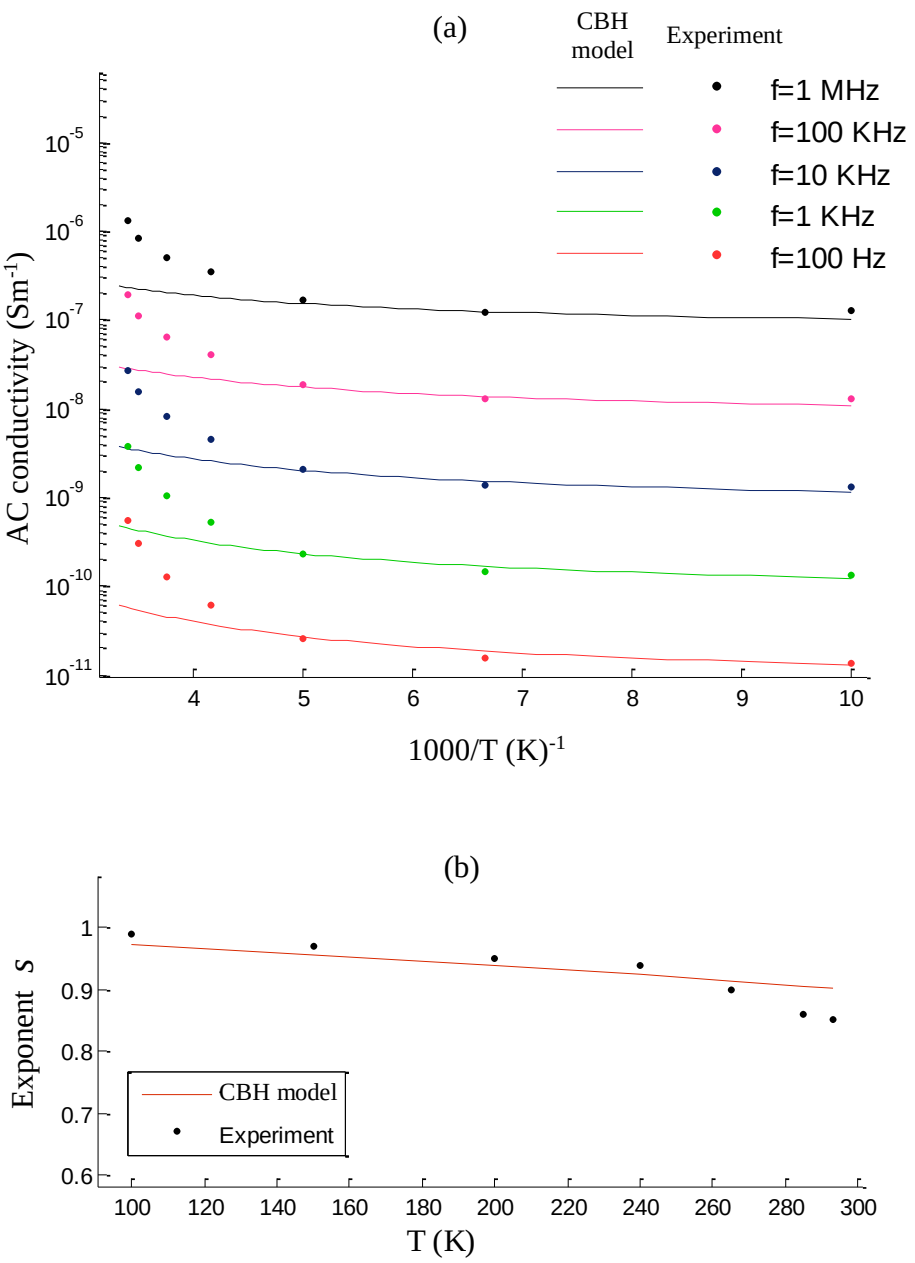

Figure 3. Fitting the CBH model to the experimental data of C_6PcH_2 device presenting by (a) temperature-dependence of the $\boldsymbol{\sigma_{AC}}$ conductivity (b) temperature-dependence of exponent *s*.

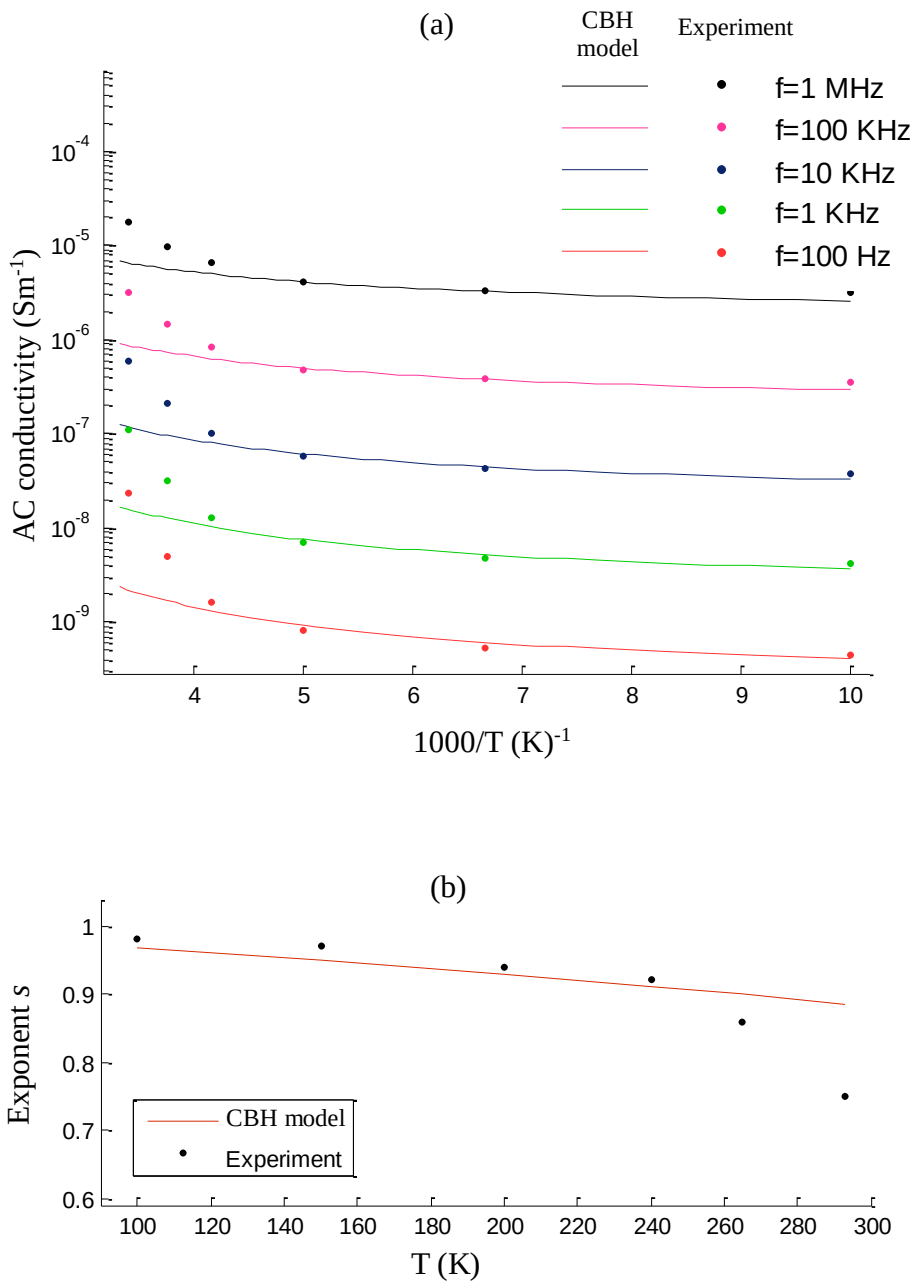

Figure 4. Fitting the CBH model to the experimental data of C_6PcH_2/PbS device presenting by (a) temperature-dependence of the AC conductivity (b) temperature-dependence of exponent *s*.

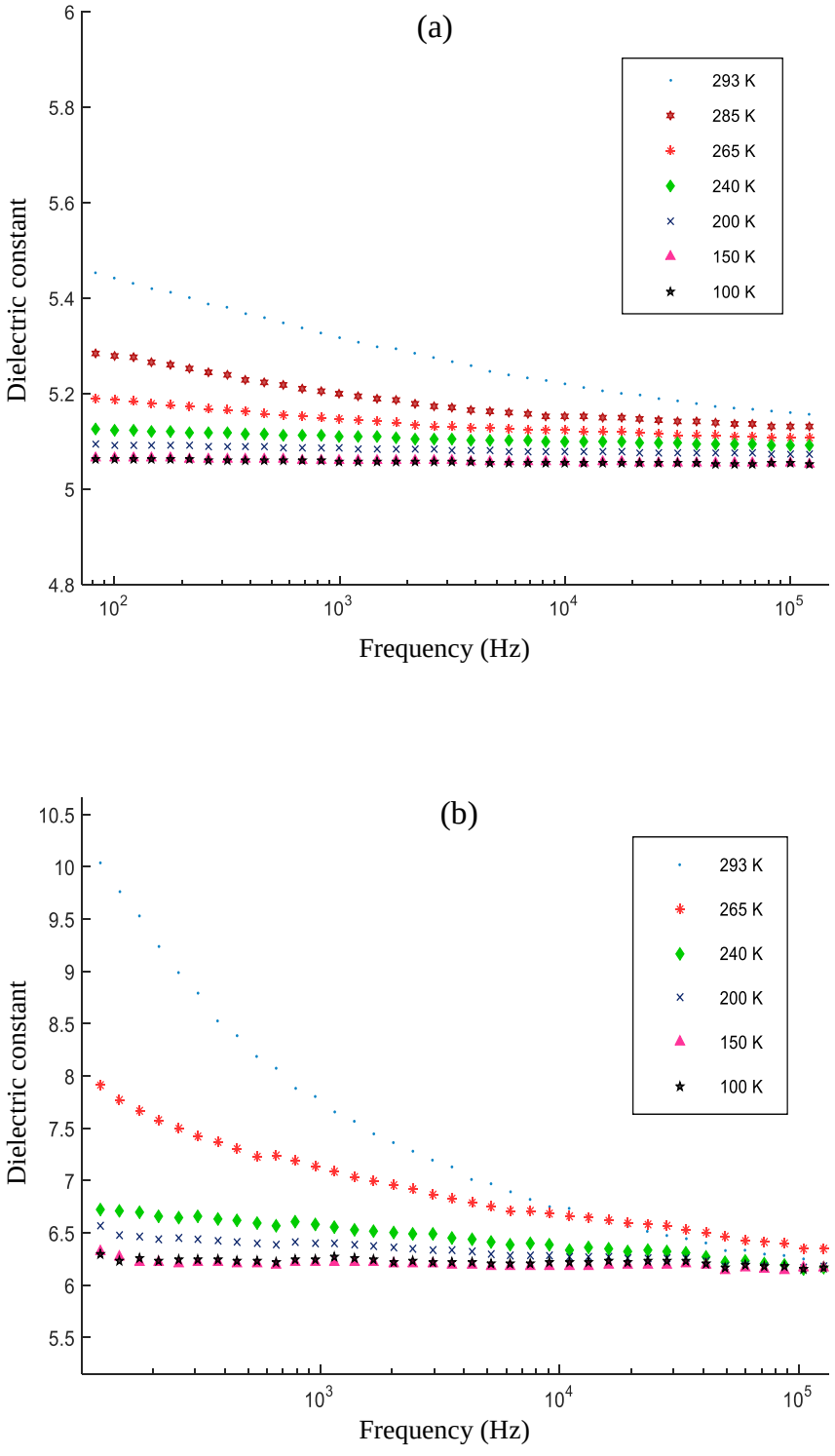

Figure 5. Frequency dispersion of dielectric constant of (a) C_6PcH_2 and (b) C_6PcH_2/PbS nanocomposite.